



T1900182169

**SUB-AUDIO MAGNETICS (SAM)**

**A High Resolution Geophysical Method for  
Simultaneously Mapping Electrical and Magnetic  
Properties of the Earth.**

By

**Malcolm K. Cattach M.Sc. (NE)**

*A Thesis Submitted for the Degree of Doctor of Philosophy  
of the University of New England*

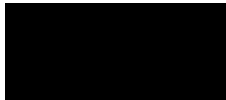
**Department of Geology and Geophysics**

**February, 1996.**

## DECLARATION

*I certify that the substance of this thesis has not already been submitted for any degree and is not currently being submitted for any other degree or qualification.*

*I certify that any help received in preparing this thesis, and all sources used, have been acknowledged in this thesis.*



*M.K. Cattach*

*Armidale,  
February, 1996.*

## DEDICATION

*I am eternally grateful for the love and support of my family.*

*This thesis is dedicated to my parents, Keith and Elwyn, my sisters, Narelle, Carol, Roslyn, Lyndell and brothers, Colin, and Peter.*

## ABSTRACT

In recent times, there has been an accelerating trend in the exploration industry towards increased spatial resolution in geophysical surveys. Rapid development in computing technology and image processing techniques has meant that much finer detail is now being observed in the data and utilised, than was previously possible. However, geophysical surveys are often very labour-intensive and therefore, expensive. Consequently, there is a need to reduce the cost of acquiring high spatial resolution data.

Developments in digital electronics have resulted in significant improvements in geophysical instrumentation. Magnetic surveys, in particular, have benefited from the advent of continuous sampling magnetometers which have made high spatial resolution or “High Definition Magnetics” (HDM) surveys both logistically and economically feasible. A review of other geophysical methods revealed that improvements in survey efficiency have not been achieved across all geophysical techniques.

Higher precision data from the electrical techniques such as electrical resistivity (ER) and electrical induced polarisation (EIP) have resulted from real-time signal processing enhancements. However, significant increases in survey efficiency were found to be restricted due to the logistical constraint imposed by the need for grounded electrodes. Similarly, improvements in survey efficiency for the electromagnetic techniques, such as, magnetometric resistivity (MMR), magnetic induced polarisation (MIP) and SIROTEM, are limited by the time-consuming requirement to precisely orientate and level the sensor prior to taking a reading.

In recognition of the potential benefits of a cost-effective means of providing detailed electrical information, a high resolution method for acquiring parameters related to the electrical properties of the earth was proposed. The method employs electric current, typically in the sub-audio frequency range of 3-200 Hz, which is induced in the ground by either galvanic or electromagnetic means using a constant-current transmitter. The electromagnetic fields produced as a result of the transmitted current flow, as well as the Earth's spatially-varying magnetic field, are monitored with an optically-pumped total field magnetometer. The method was consequently entitled “Sub-Audio Magnetics” (SAM).

Spectral analysis of the magnetic field changes allows a suite of geophysical parameters to be derived. In order to differentiate the electrical measurements so obtained, from parameters recorded by conventional methods, new terminology was introduced. Where galvanic induction is used the properties measured include “Total Field MagnetoMetric Resistivity” (TFNMR) and “Total Field MagnetoMetric Induced Polarisation” (TFMMIP). The term “Total Field ElectroMagnetics” (TFEM) was adopted as the property measured during surveys which employ electromagnetic induction. Each of the parameters may be measured at close sample intervals while continuously traversing either on foot or in a ground or airborne vehicle. A significant benefit of the method in terms of survey efficiency, is the simultaneous acquisition of High Definition Magnetics (HDM).

In order to demonstrate the SAM concept, a series of feasibility trials using galvanic induction were conducted over known geology using a state-of-the-art, TM-4 caesium vapour magnetometer as the receiver. Analysis of the recorded waveforms confirmed the technical viability of the technique and enabled signal strengths to be quantified. Data reduction procedures were developed to correct the TFMMR data for the electromagnetic field due to current flowing in the wire feeding the electrodes as well as to perform normalisation for the expected response over a homogeneous half-space. The higher spatial resolution was found capable of providing significantly more diagnostic information than possible using conventional electrical or electromagnetic methods.

Deficiencies in the instrumentation used for the feasibility trials were addressed through the development of a TM-4 option card (the SAMCard) which featured:

- Measurement resolution of the order of 0.02 nT.
- A bandwidth of 500 Hz to prevent aliasing of the higher frequency components.
- Constant sample interval to enable waveform averaging and data processing.
- GPS synchronisation between the receiver and the transmitter to facilitate the detection of polarity reversals and to quantify phase lags from the transmitted signal.
- Separation of the spatially-varying field from the time-varying field due to the transmitted current.
- Sample intervals for the electromagnetic parameters of down to 2 m.

A series of field trials of the prototype SAMCard-enhanced TM-4 demonstrated that the simultaneous acquisition of HDM and TFMMR was readily achieved. However, characterisation of the much weaker TFMMIP response was not successful due to remaining deficiencies in instrument design. The results of the field trials enabled future development strategies for attaining TFMMIP information to be proposed.

The Sub-Audio Magnetics method is now being operated commercially for the acquisition of HDM and TFMMR. Exploration surveys have demonstrated the benefits both of multiple-property data sets and of high resolution for all parameters. In some situations, the TFMMR data were found to supplement the magnetics by providing consistent information which confirmed and extended the interpretation of the magnetics. In other cases, the TFMMR data exposed new, yet contrasting information which complemented the magnetics. The surveys highlighted the greater diagnostic power which can be derived from having multiple data sets as well as the interpretational bias which may result from too much dependence on a single data type.

Because of its inherent cost-efficiency and superior spatial resolution, Sub-Audio Magnetics has the potential to significantly enhance geophysical mapping for mineral exploration, archaeological investigation and environmental studies of salinity, industrial waste and chemical contamination in soils.

## ACKNOWLEDGEMENTS

I wish to express my sincere thanks to my colleague and supervisor, Dr J.M. Stanley (Director, Geophysical Research Institute, UNE), for his inspiration, encouragement and academic guidance throughout this research project.

This study was made possible through the significant financial and logistical support provided by Normandy Exploration Ltd., to whom I'm extremely grateful. My special thanks go to Mr G.W. Boyd (Chief Research Geophysicist, Normandy Exploration), for his long-term friendship, commitment and confidence in the project.

This study was completed on a part-time basis over a five year period whilst I was employed by the Geophysical Research Institute, UNE. I feel very honoured to have shared in the growth and success of the Institute over the last ten years and am very appreciative of the friendship and support offered by my colleagues. In particular, I would like to acknowledge the significant technical input provided by the following GRI staff:

- Mr S.J. Lee (Systems Engineer) whose skills were responsible for engineering the TM-4 magnetometer, without which this project could not have been attempted.
- Mr R.C. Bradbury (Senior Electronics Engineer) who designed and implemented the SAMCard and with whom I had many valued discussions.
- Mr D.J. McCarthy (Electronics Engineer) for his assistance in developing the SAM-XMT transmitter controller.
- Mr D.B. Boggs (Geophysicist and fellow Ph.D. student) for his considerable energy and assistance with much of the field work as well as the development of some of the SAMCard processing software.
- Mr P.J. Clark (Senior Geophysicist) for many valued discussions as well as his on-going friendship and support.
- Dr J. Zhou (Senior Research Geophysicist and fellow Ph.D. student) for his mathematical expertise and companionship during some very late nights.

I am also indebted to the numerous GRI staff members and students who, at different times, assisted (some voluntarily) with the often arduous and frustrating field work. I am particularly grateful to Mr J.P. Wilkie-Snow, Mr B. Payne, Mr M.W. Donaldson, Mr D.A. Mack, Mr N. Fathianpour, Ms M.L. Laffan, Mr D.C. Lawie, Mr G.L. Landsberg and Mr M.J. Maticka.

I would like to thank those mining companies who have been prepared to trial SAM. The trials have proven invaluable to our understanding of the technique. In particular, I would like to thank Mr S.N. Sheard and Mr T. Ritchie from MIM Exploration, Mr P. Williams and Ms L.J. Vella from Western Mining Corporation, Mr K. Jones from

Ashton Mining and Mr D.F. Larsen from Pasminco Mining for their support and permission to present the results of some of those surveys in this thesis.

My sincere thanks also go to Mrs R.G. Stanley and Mr S.M. Griffin for their meticulous attention to detail in proof-reading this thesis.

As anyone who has undertaken a part-time research degree would appreciate, this project has placed an enormous amount of pressure on my family. This thesis could not have been completed, if not for the boundless support offered by my wife, Fongue and my daughters, Samantha (SAM) and Ellen who, to this day, haven't known a father who wasn't always working. I thank them sincerely, for their love, understanding and never-ending patience.

# TABLE OF CONTENTS

<b>Declaration</b> .....	<b>ii</b>
<b>Dedication</b> .....	<b>iii</b>
<b>Abstract</b> .....	<b>iv</b>
<b>Acknowledgements</b> .....	<b>vi</b>
<b>Table of Contents</b> .....	<b>viii</b>
<b>List of Figures</b> .....	<b>xiii</b>
<b>List of Plates</b> .....	<b>xiv</b>
<b>List of Tables</b> .....	<b>xviii</b>
<b>List of Symbols</b> .....	<b>xix</b>
<b>List of Acronyms</b> .....	<b>xx</b>
<b>1 INTRODUCTION</b> .....	<b>1</b>
1.1 An Endeavour to Increase the Spatial Resolution and Interpretability of Geophysical Surveys .....	1
1.2 Project Objectives .....	4
1.3 Achievements of the Research .....	6
1.4 Organisation of the Thesis .....	7
<b>2 REVIEW OF RELEVANT CONTEMPORARY GEOPHYSICAL SURVEY METHODS</b> .....	<b>9</b>
2.1 Introduction .....	9
2.2 State-of-the-Art High Definition Magnetics .....	10
2.2.1 Field Procedure .....	12
2.2.2 Instrumentation .....	13
2.3 Contemporary Galvanic Electrical Methods .....	14
2.3.1 Electrical Resistivity (ER) .....	14
2.3.1.1 Field Procedure .....	15
2.3.1.2 Instrumentation .....	17
2.3.1.3 Measured Parameters .....	19
2.3.2 The Electrical Induced Polarisation (EIP) Method .....	19
2.3.2.1 Field Procedure .....	20
2.3.2.2 Instrumentation .....	20
2.3.2.3 Measured Parameters .....	21
2.3.3 Magnetometric Resistivity (MMR) .....	25
2.3.3.1 Field Procedure .....	27
2.3.3.2 Instrumentation .....	28
2.3.3.3 Measured Parameters .....	29
2.3.3.4 Corrections .....	29



2.3.4	The Magnetic Induced Polarisation (MIP) Method .....	31
2.3.4.1	Field Procedure .....	32
2.3.4.2	Instrumentation .....	34
2.3.4.3	Measured Parameters .....	34
2.4	Comparison of the EIP and MIP Methods .....	35
2.5	Discussion .....	39
<b>3</b>	<b>THE SUB-AUDIO MAGNETICS CONCEPT.....</b>	<b>40</b>
3.1	Introduction .....	40
3.2	SubAudio Magnetics .....	42
3.2.1	Survey Speed .....	42
3.2.2	TFMMR / TFMMIP .....	43
3.3	Components of the SAM Signal .....	44
3.3.1	Calculation of the Primary Field .....	45
3.3.2	Calculation of the Normal Field .....	46
3.4	Determination of Total Field Corrections .....	47
3.5	Analytical Solutions for Total Field Magnetometric Resistivity (TFMMR) .....	52
3.6	Factors Affecting Data Quality .....	54
3.6.1	The Earth's Ambient Electromagnetic Field .....	54
3.6.2	Electromagnetic Induction (EMI Coupling) .....	57
<b>4</b>	<b>FEASIBILITY STUDIES: INSTRUMENTATION AND FIELD PROCEDURE.....</b>	<b>58</b>
4.1	Introduction .....	58
4.2	The Geophysical Technology, Model TM-4 Caesium Vapour Magnetometer .....	59
4.2.1	The TM-4 Data Acquisition and Control Unit .....	59
4.2.2	Optically-Pumped Magnetometer Sensors .....	60
4.2.2.1	The Principle of Optical Pumping .....	62
4.2.2.2	The Phenomenon of Unequal Pumping .....	65
4.2.2.3	The Effect of Sensor Orientation .....	67
4.2.2.4	Performance Characteristics of Optically-pumped Magnetic Sensors .....	68
4.2.3	The TM-4 Frequency Counter .....	69
4.3	Transmitter - Zonge GGT-10 .....	70
4.4	Base-Station Magnetometer - Geometrics G-856 .....	70
4.5	Field Procedure .....	70
<b>5</b>	<b>FEASIBILITY STUDIES: WAVEFORM INVESTIGATION AND DATA REDUCTION.....</b>	<b>75</b>
5.1	Introduction .....	75
5.2	Parameters of the SAM Waveform .....	75
5.3	Investigation of the Recorded Waveforms .....	77
5.3.1	Waveform Types .....	77
5.3.2	The Effect of Superposition of $H_{primary}$ and $H_G$ .....	79
5.3.2.1	In-Phase Signals .....	79
5.3.2.2	Out-Of-Phase Signals .....	80

5.4 Data Reduction Procedures .....	82
5.4.1 Extraction of $H_S$ and $H_{Mod}$ from $H_T$ .....	82
5.4.2 Correction of $H_S$ for Temporal Variation .....	83
5.4.3 Extraction of TFMMR Information .....	83
5.4.4 Correction for $H_{Primary}$ and $H_{Normal}$ .....	84
5.4.5 Extraction of TFMMIP Parameters .....	85
5.5 Data Quality .....	87
5.5.1 The Effect of High Frequency High Amplitude Noise Resulting from the Spatially-varying Magnetic Field .....	88
5.5.2 The Effect of EM Coupling .....	88
5.5.3 The Effect of Mains Power Interference .....	88
5.6 Discussion .....	89
<b>6 FEASIBILITY STUDIES - FIELD RESULTS.....</b>	<b>92</b>
6. Introduction.....	92
6.2 Feasibility Study #1 - Orlando Deposit, Tennant Creek, Northern Territory .....	93
6.2.1 Location.....	93
6.2.2 Geological Setting .....	94
6.2.2.1 Form of the Mineralisation .....	96
6.2.3 Prior Geophysics .....	98
6.2.3.1 Magnetics .....	98
6.2.3.2 Gradient Array Induced Polarisation (IP).....	100
6.2.4 SAM Field Procedure.....	102
6.2.5 Results .....	104
6.2.5.1 Total Magnetic Intensity .....	104
6.2.5.2 Total Field Magnetometric Resistivity (TFMMR).....	107
6.3 Feasibility Study #2 - Flying Doctor Deposit, Broken Hill, New South Wales .....	111
6.3.1 Location.....	111
6.3.2 Geological Setting .....	112
6.3.2.1 Form of the Mineralisation .....	115
6.3.3 Prior Geophysics .....	116
6.3.3.1 Induced Polarisation (IP / Resistivity).....	116
6.3.3.2 Magnetic Induced Polarisation (MIP).....	119
6.3.4 SAM Field Procedure.....	120
6.3.5 Results .....	122
6.3.5.1 Total Magnetic Intensity (TMI).....	122
6.3.5.2 Total Field Magnetometric Resistivity (TFMMR).....	122
6.4 Evaluation of the Feasibility Trials .....	125
<b>7 DEVELOPMENT OF A PROTOTYPE SAM RECEIVER.....</b>	<b>126</b>
7.1 Introduction.....	126
7.2 Specifications of a Sub-Audio Magnetics Receiver.....	127
7.2.1 Requirements for the Determination of the Spatially-varying Magnetic Field, $H_S$ .....	127

7.2.2 Requirements for the Determination of the SAM Signal, $H_{Mod}$ .....	127
7.3 The Approach Used .....	129
7.3.1 Total Magnetic Field Measurements .....	129
7.3.2 The SAM Measurements - The SAMCard .....	130
7.3.2.1 The Demodulation Circuit .....	130
7.3.2.2 Removal of Low Frequency Noise .....	130
7.3.2.3 Anti-Aliasing Filter .....	130
7.3.2.4 Mains Power Filters .....	132
7.3.2.5 Analogue to Digital Conversion .....	132
7.3.2.6 Transmitter - Receiver Synchronisation .....	132
7.4 TM-4 Enhancements .....	134
7.5 The SAM-XMT Transmitter Controller .....	137
7.6 The SAM Signal Simulator .....	139
7.7 Data Processing .....	141
7.7.1 Correction for the SAMCard Filter Response .....	142
7.7.2 Slope correction .....	144
7.7.3 Calculation of parameters .....	144
7.7.3.1 Corrections for TFMMR Parameters .....	144
7.7.3.2 Corrections for TFMMIP Parameters .....	145
7.7.4 Conclusion .....	146

## **8 FIELD TRIALS OF THE PROTOTYPE SAM RECEIVER .....147**

8.1 Introduction .....	147
8.2 SAM Case Study #1 - Taronga Tin Deposit, Emmaville, NSW .....	148
8.2.1 Location .....	148
8.2.2 Geological Setting .....	150
8.2.2.1 Form of the Mineralisation .....	153
8.2.3 Prior Geophysics .....	155
8.2.4 SAM Field Procedure .....	157
8.2.5 Results .....	159
8.2.5.1 Total Magnetic Intensity (TMI) .....	159
8.2.5.2 Total Field Magnetometric Resistivity (TFMMR) .....	161
8.2.5.3 Total Field Magnetometric Induced Polarisation (TFMMIP) .....	163
8.2.6 The Effect of Topography on Primary Field Corrections .....	165
8.2.7 Discussion .....	167
8.3 Case Study #2 - HYC Deposit, Mc Arthur River, Northern Territory .....	169
8.3.1 Location .....	169
8.3.2 Geological Setting .....	170
8.3.2.1 Mineralisation .....	171
8.3.3 Prior Geophysics .....	172
8.3.4 SAM Field Procedure .....	175
8.3.5 Results .....	177

8.3.5.1 Total Magnetic Intensity (TMI).....	177
8.3.5.2 Total Field Magnetometric Resistivity (TFMMR).....	177
8.3.5.3 Total Field Magnetometric Induced Polarisation (TFMMIP).....	180
8.3.6 Discussion.....	180
8.4 Case Study #3 - Homogeneous Half-Space, McArthur River, Northern Territory.....	182
8.4.1 Location.....	182
8.4.2 SAM Field Procedure.....	182
8.4.3 Results.....	184
8.4.3.1 Total Magnetic Intensity (TMI).....	184
8.4.3.2 Total Field Magnetometric Resistivity (TFMMR).....	184
8.4.4 Discussion.....	185
8.5 Conclusions.....	190
8.5.1 Assessment of the Prototype SAM Receiver for the Determination of Total Magnetic Intensity, TMI.....	190
8.5.2 Assessment of the Prototype SAM Receiver for the Determination of TFMMR and TFMMIP.....	190
<b>9 EXPLORATION EXAMPLES.....</b>	<b>193</b>
9.1 Introduction.....	193
9.2 Supplementary Data Sets.....	194
9.3 Complementary Data Sets.....	197
9.4 Discussion.....	201
<b>10 PROJECT REVIEW, EVALUATION AND CONCLUSION.....</b>	<b>203</b>
10.1 Introduction.....	203
10.2 Project Review.....	205
10.2.1 Stage 1 - Conceptual Development.....	205
10.2.2 Stage 2 - Field Tests Using Existing Instrumentation.....	207
10.2.3 Stage 3 - Instrument Development and Field-Testing.....	207
10.3 Recommendations for Future Development and Related Research.....	209
10.3.1 Proposed Further SAM Receiver Development.....	209
10.3.1.1 The “Intelligent” Frequency Counter.....	211
10.3.1.2 The Data Logger.....	212
10.3.2 Alternative Sensors.....	212
10.3.3 Field Procedure Modifications.....	213
10.3.4 Alternative Applications of SAM.....	214
10.3.5 Related Theoretical Research.....	214
10.4 Project Evaluation and Conclusions.....	214
<b>References.....</b>	<b>219</b>
<b>Research Related Awards.....</b>	<b>227</b>

## LIST OF FIGURES

Figure 2-1.	Common Resistivity Arrays (After Sumner, 1976).....	18
Figure 2-2.	The time domain IP waveforms showing the transmitted current waveform and the received voltage waveform. (After Sumner, 1979).....	22
Figure 2-3.	IP Frequency domain waveforms, showing a controlled, constant inducing current $I$ being detected as voltages $V_1$ and $V_2$ where $V_1 < V_2$ . (After Sumner, 1979).....	22
Figure 2-4.	Timing for the integration windows for a Scintrex IPR-12 IP receiver (After Scintrex, 1993b). .....	23
Figure 2-5.	IP phase determination and vector components (After Sumner, 1976). .....	26
Figure 2-6.	The x-component of the Normal magnetic field due to current flow between a pair of electrodes located on the y-axis and separated by a distance $L$ . (After Edwards and Nabighian, 1991). .....	31
Figure 2-7.	Typical MIP horseshoe array for reconnaissance surveying (After Seigel and Howland-Rose, 1990).....	33
Figure 2-8.	Typical MIP linear array for detailed surveying (After Seigel and Howland-Rose, 1990). ....	33
Figure 2-9.	The EIP and MIP Energisation Process (After Howland-Rose, 1980). .....	37
Figure 2-10.	The EIP and MIP Discharge of Induced Polarisation (After Howland-Rose, 1980). .....	37
Figure 3-1.	Layout of a typical TFMMR / TFMMIP survey showing the ideal electrode positions and survey orientation relative to the direction of geological strike. Current electrode positions are $C_1$ and $C_2$ .....	44
Figure 3-2.	Ampere's Law - A current $I$ passing through a length of conductor $\Delta l$ creates a magnetising field $\Delta H$ at a point $P$ (Drawn from Telford <i>et al.</i> , 1990). .....	46
Figure 3-3.	Elements of the Earth's magnetic field with respect to a local coordinate system. ....	48
Figure 3-4.	Projection of an applied field $F_A$ onto a unit vector defining the direction of the Earth's magnetic field $F_E$ . .....	49
Figure 3-5.	The theoretical Primary field ( $H_{Primary}$ ) as measured with a total field magnetometer, resulting from current flowing through cables feeding grounded electrodes at positions $C_1$ and $C_2$ . .....	50
Figure 3-6.	The theoretical Normal field ( $H_{Normal}$ ) as measured with a total field magnetometer due to current flowing through a homogeneous earth.....	51
Figure 3-7.	Geometry used to define a vertical fault model separating two media with different resistivities (After Fathianpour and Cattach, 1995). .....	52
Figure 3-8.	Horizontal X, Y and vertical Z components of the anomalous magnetic field for the vertical fault model. Notice the relative magnitude of the -Z component compared to those of the horizontal component (After Fathianpour and Cattach, 1995).....	53
Figure 3-9.	Profiles showing the influence of the geomagnetic field inclination on TFMMR measurements for a fixed declination of $25^\circ$ (After Fathianpour and Cattach, 1995). .....	53
Figure 3-10.	Profiles showing the influence of the geomagnetic field declination on TFMMR measurements for a fixed inclination of $60^\circ$ (After Fathianpour and Cattach, 1995). .....	54
Figure 3-11.	Components of the electromagnetic noise spectrum (After Macnae <i>et al.</i> , 1984).....	55
Figure 4-12.	Caesium-vapour magnetometer schematic (After Dobrin, 1976).....	64
Figure 4-13.	Energy levels of the caesium-133 isotope showing Hyperfine splitting ("F") levels and Zeeman splitting ("m") levels (After Varian Associates of Canada, 1977). .....	64
Figure 4-14.	(a) The spectrum of electron transitions between $F = 4$ Zeeman levels in an equilibrium caesium atom subject to an ambient magnetic field of 50000 nT. (b) The hyperfine	

	spectrum when subjected to $\Delta m_F = +1$ pumping radiation. (c) The hyperfine spectrum when subjected to $\Delta m_F = -1$ pumping radiation. (After Meilleroux, 1969).....	66
Figure 4-15.	Operating orientations for the Scintrex CS-2 sensor showing both equatorial and polar dead zones (After Scintrex, 1993a).....	67
Figure 5-1.	A ten second time sample (15 m traverse length) illustrating the artificially induced modulation, $H_{Mod}$ , superimposed on the spatially-varying magnetic field, $H_S$ .....	77
Figure 5-2.	Examples of recorded waveforms for a one second time interval. (A) Typical square waves. (B) Spikes. (C) Square waves with spikes.....	78
Figure 5-3.	The effect of superposition of $H_{Primary}$ and $H_G$ (8 Hz, 100% duty cycle) for in-phase signals.....	80
Figure 5-4.	The effect of superposition of $H_{Primary}$ and $H_G$ (8 Hz, 100% duty cycle) with a phase lag of 50 mrad.....	81
Figure 5-5.	(A) A sample raw data profile $H_T$ recorded over a conductor. The component signals were separated by digital filtering to produce: (B) The spatially-varying magnetic field data $H_S$ , and (C) The SAM signal $H_{Mod}$ .....	82
Figure 5-6.	(A) Peak amplitude of the SAM modulation $H_{Pk}$ determined from the data in Figure 5-5. (B) The calculated Primary Field $H_{Primary}$ . (C) The calculated Normal Field $H_{Normal}$ . (D) The Normalised TFMMR data $H_N$ .....	84
Figure 5-7.	Normalised Amplitude spectrum of a 1024 point SAM signal showing the fundamental frequency and the odd harmonics. The harmonics above the 11 <sup>th</sup> have been folded back about the Nyquist frequency due to aliasing.....	86
Figure 5-8.	Relative amplitude of the 3 <sup>rd</sup> harmonic and the fundamental frequency calculated from the data in Figure 5-5.....	87
Figure 5-9.	Recorded waveform showing 50 Hz mains power interference.....	89
Figure 6-10.	Orlando Location Plan (After Oates, 1993).....	94
Figure 6-11.	Orlando Regional Geology (After Foley <i>et al.</i> , 1995).....	95
Figure 6-12.	Orlando Local Geology Map (Drawn from Oates, 1993).....	97
Figure 6-13.	Orlando Geological Section - Line 70C mE (After Foley <i>et al.</i> , 1995).....	98
Figure 6-14.	Contours of the vertical component of the magnetic field in gammas (nT). Orlando Mine area (Drawn From McNeil, 1966).....	99
Figure 6-15.	Orlando Aeromagnetic Data (After Foley <i>et al.</i> , 1995).....	99
Figure 6-16.	Gradient Array IP contours (After Foley <i>et al.</i> , 1995).....	101
Figure 6-17.	Layout of the Survey Area showing the locations of electrodes C1, C2, C3 and C4 and current-bearing wire.....	103
Figure 6-18.	Orlando - Total Magnetic Intensity, $H_S$ , with geological overlay.....	105
Figure 6-19.	Orlando - Total Magnetic Intensity, $H_S$ - Reduced to the Pole.....	106
Figure 6-20.	Orlando - Normalised TFMMR, $H_N$ with geological overlay.....	109
Figure 6-21.	Normalised TFMMR, $H_N$ - Reduced to Pole.....	110
Figure 6-22.	Locality and Regional Setting for Broken Hill (After Stevens <i>et al.</i> , 1980).....	111
Figure 6-23.	Flying Doctor Geological Plan (Drawn From Larsen, 1993).....	113
Figure 6-24.	Flying Doctor Geological Sections (Drawn From Tyne, 1985).....	114
Figure 6-25.	Gradient Array Resistivity and Induced Polarisation Survey. Flying Doctor Prospect (After Tyne, 1987).....	117
Figure 6-26.	Dipole-dipole resistivity and IP profile - Line 25.25 S. Flying Doctor Prospect (After Tyne, 1987).....	118
Figure 6-27.	Time domain MIP response - Line 25.25 S (After Bishop, 1989).....	119
Figure 6-28.	Frequency domain MIP response - Line 25.25 S (After Bishop, 1989).....	120
Figure 6-29.	Layout of the Survey Area showing the location of the electrodes and current-bearing wire.....	121

Figure 6-30.	Flying Doctor - Total Magnetic Intensity, $H_S$ with geological overlay.....	123
Figure 6-31.	Flying Doctor - Normalised TFMMR, $H_N$ .....	123
Figure 6-32.	Flying Doctor TFMMR, $H_N$ - Reduced to Pole.....	124
Figure 6-33.	Flying Doctor First Vertical Derivative of TFMMR, $H_N$ - RTP.....	124
Figure 7-1.	Schematic of the SAMCard (After Bradbury, 1994a).....	131
Figure 7-2.	(A) Unstacked, 1024 point waveform recorded from the SAM signal simulator without SAM modulation, and (B) The amplitude spectrum of the waveform in (A) (After Bradbury, 1994a).....	136
Figure 7-3.	(A) Stacked, 1024 point waveform recorded from the SAM signal simulator without SAM modulation, showing the effect of 8x stacking, and (B) The amplitude spectrum of the waveform in (A) (After Bradbury, 1994a).....	136
Figure 7-4.	Larmor Signal Generator Schematic (After Bradbury, 1994b).....	140
Figure 7-5.	(A) Amplitude response, and (B) Phase response of the SAMCard (After Bradbury, 1994a).....	142
Figure 7-6.	(A) Typical SAMCard recording of a square wave produced by the SAM signal generator showing distortion due to the SAMCard's filter response, and (B) The result of correction of the recorded data by applying the compensation filter (After Bradbury, 1994a).....	143
Figure 7-7.	Diagram showing the phase relationship between $H_{Primary}$ , $H_G$ and $H_{Mod}$ .....	145
Figure 8-1.	Taronga District Map (After Newmont Holdings Pty Ltd, 1982).....	149
Figure 8-2.	Taronga Tin Project Regional Geology (After Newmont Holdings Pty Ltd, 1982).....	151
Figure 8-3.	Taronga Tin Project District Geology (After Newmont Holdings Pty Ltd, 1982).....	152
Figure 8-4.	Taronga Southern Zone Mineralisation (Drawn From Newmont Holdings Pty Ltd, 1982).....	154
Figure 8-5.	Geological Cross Section - Line 3525 mN (Drawn From Newmont Holdings Pty Ltd, 1982).....	155
Figure 8-6.	Taronga - dipole-dipole array IP pseudosection from Line 3525N (Drawn From Cattach, 1985).....	156
Figure 8-7.	Schematic showing the layout of the electrodes and their feeding wires with respect to the survey area.....	157
Figure 8-8.	The location of the survey area and current-carrying wire with respect to topography.....	158
Figure 8-9.	Taronga - Total Magnetic Intensity, $H_S$ .....	160
Figure 8-10.	Taronga - TMI - Upward continued to 25 m.....	160
Figure 8-11.	Taronga - Normalised TFMMR, $H_N$ .....	162
Figure 8-12.	Taronga - Normalised TFMMR, $H_N$ , Reduced to Pole.....	162
Figure 8-13.	Taronga - First Vertical Derivative of $H_N$ - Reduced to Pole.....	164
Figure 8-14.	Taronga - Corrected Phase Response.....	164
Figure 8-15.	Diagram illustrating the effect of elevation on the strength and direction of the magnetic field due to current flowing in a long straight wire.....	166
Figure 8-16.	The difference in the Primary correction calculated with and without consideration of elevation.....	168
Figure 8-17.	TFMMR corrected for the Primary field with topographic correction.....	168
Figure 8-18.	Location and Geological Map of the Eastern Batten Trough in the McArthur River Area. Hatched area is surface projection of the HYC deposit. (After Logan <i>et al.</i> 1990).....	170
Figure 8-19.	Geological cross-sections looking north (Profile A-B) and looking west (Profile C-D) through the HYC deposit (After Logan <i>et al.</i> 1990).....	171
Figure 8-20.	Electrodes and cable configurations of the MIP survey over the HYC deposit (After Hishida <i>et al.</i> , 1993).....	173
Figure 8-21.	Normalised horizontal magnetic field ( $H_N$ ) contours (%) for current flow parallel to strike over the HYC deposit (After Hishida <i>et al.</i> , 1993).....	174

Figure 8-22.	Relative Phase Shift (RPS) contours ( $^{\circ}$ ) for current flow parallel to strike over the HYC deposit (After Hishida <i>et al.</i> , 1993).....	175
Figure 8-23.	Schematic showing the layout of the electrodes and current carrying wire with respect to the survey area.....	176
Figure 8-24.	HYC - Total Magnetic Intensity, $H_S$ .....	179
Figure 8-25.	HYC - Normalised TFMMR, $H_N$ .....	179
Figure 8-26.	Schematic showing the layout of the electrodes with respect to the survey area.....	183
Figure 8-27.	Total Magnetic Intensity, $H_S$ .....	186
Figure 8-28.	Homogeneous Half-Space - MI, $H_S$ - Jpward Continued 20 m.....	186
Figure 8-29.	Homogeneous Half-Space - Peak amplitude of $H_{Mod}$ , $H_{Pk}$ .....	187
Figure 8-30.	Homogeneous Half-Space - Theoretical Primary field, $H_{Primary}$ .....	187
Figure 8-31.	Homogeneous Half-Space - Ground field, $H_G$ .....	188
Figure 8-32.	Homogeneous Half-Space - Theoretical Normal field, $H_{Normal}$ .....	188
Figure 8-33.	Homogeneous Half-Space - Normalised TFMMR, $H_N$ .....	189
Figure 9-1.	Archaean Gold Prospect: Grid A - Total Magnetic Intensity, $H_S$ .....	195
Figure 9-2.	Archaean Gold Prospect: Grid A - Normalised TFMMR, $H_N$ .....	195
Figure 9-3.	Archaean Gold Prospect: Grid B - Total Magnetic Intensity, $H_S$ .....	196
Figure 9-4.	Archaean Gold Prospect: Grid B - Normalised TFMMR, $H_N$ .....	196
Figure 9-5.	Cu/Au Prospect: Grid C - Total Magnetic Intensity, $H_S$ .....	198
Figure 9-6.	Cu/Au Prospect: Grid C - Normalised TFMMR, $H_N$ .....	198
Figure 9-7.	Cu/Au Prospect: Grid D - Total Magnetic Intensity, $H_S$ .....	200
Figure 9-8.	Cu/Au Prospect: Grid D - Normalised TFMMR, $H_N$ .....	200
Figure 10-1.	The proposed SAM Capable Magnetometer System - Design Concept.....	210



## LIST OF PLATES

Plate 4-1. The TM-4 magnetometer controller showing the in-built cotton-thread odometer. ....	61
Plate 4-2. The EG&G Geometrics G-822A caesium vapour magnetic sensor. ....	61
Plate 4-3. The Zonge GGT-10 IP/EM Transmitter. ....	71
Plate 4-4. The Zonge XMT-16 Transmitter Controller. ....	71
Plate 4-5. The Kohler Motor-Generator and Zonge VR-1 Voltage Regulator. ....	72
Plate 4-6. The Zonge VR-1 Voltage Regulator. ....	72
Plate 4-7. The TM-4 magnetometer system in hand-held configuration showing a single Geometrics G-822A sensor. ....	74
Plate 7-8. The TM-4 based SAM Receiver showing the mounting position of the Trimble SVeeSix GPS Receiver. ....	138
Plate 7-9. The SAM controller incorporating the Trimble SVeeSix GPS Receiver. ....	138

## LIST OF TABLES

Table 4-1.	The TM-4 Controller Technical Specifications. (After Geophysical Technology Pty Ltd, 1990).....	60
Table 4-2.	TM-4 Frequency Counter specifications (20 MHz reference clock) at ambient magnetic field values of 50000 and 60000 nT (After Lee, 1987). .....	69
Table 5-1.	The naming convention and symbols used to describe the components of the SAM waveform.....	76
Table 7-1.	Specifications of the SAM-XMIT Transmitter Controller (After McCarthy, 1994).....	137
Table 7-2.	Specifications of the SAM Signal Simulator (After Bradbury, 1994b). .....	141
Table 10-1.	Survey specifications and data acquisition rates for SAM, EIP and MIP. ....	216
Table 10-2.	Data acquisition costs for SAM, EIP and MIP surveys. ....	217

# LIST OF SYMBOLS

## Greek Symbols

$\rho$	resistivity
$\rho_a$	apparent resistivity
$\beta$	phase angle
$\pi$	pi
$\eta$	Planck's constant

## Roman Symbols

$C_1, C_2$	current electrodes
$D$	declination of earth's magnetic field
$E$	the Zeeman energy difference
$f_{Max(Spatial)}$	maximum spatial frequency in magnetic profile
$f_{Max(Time)}$	maximum time-varying frequency of spatial origin due to traverse speed
$\mathbf{F}_E$	unit vector defining direction of earth's magnetic field
$G$	geometric factor
$h$	height of sensor above ground
$H_G$	Ground magnetic field
$H_{Mod}$	Modulation in the magnetic field due to transmitted signal
$H_N$	Normal magnetic field
$H_{Norm}$	normalised magnetic field
$H_P$	primary magnetic field (analogous to $V_P$ )
$H_{Primary}$	Primary magnetic field due to current flow in current-bearing wires
$H_{Pk}$	Peak amplitude of SAM modulation
$H_S$	spatially-varying magnetic field
$H_T$	total magnetic field
$I$	inclination of Earth's magnetic field
$I$	current
$I_P$	primary current
$M$	chargeability
$M_i$	$i$ th chargeability integration window
$P_1, P_2$	potential electrodes
$t_1, t_2$	times at beginning and end of integration window
$V$	velocity
$V$	voltage
$V_P$	primary voltage
$V_t$	voltage at time $t$
$X_E, Y_E, Z_E$	x,y,z-components of unit vector defining the earth's magnetic field

## LIST OF ACRONYMS

AC	Alternating Current
AFMAG	Audio Frequency MAGnetics
AMT	Audio MagnetoTellurics
ASEG	Australian Society of Exploration Geophysicists
CSAMT	Controlled Source Audio MagnetoTellurics
DC	Direct Current
DHMMR	Downhole MagnetoMetric Resistivity
EIP	Electrical Induced Polarisation
ELF	Extremely Low Frequency
EM	ElectroMagnetic
ER	Electrical Resistivity
FE	Frequency Effect
GPS	Global Positioning System
GRI	Geophysical Research Institute
HDM	High Definition Magnetics
IP	Induced Polarisation
MIP	Magnetic Induced Polarisation
MMR	MagnetoMetric Resistivity
MT	MagnetoTellurics
PFE	Percent Frequency Effect
RF	Radio Frequency
RPS	Relative Phase Shift
SAM	Sub-Audio Magnetics
SP	Self Potential
TFEM	Total Field ElectroMagnetics
TFMMIP	Total Field MagnetoMetric Induced Polarisation
TFMMR	Total Field MagnetoMetric Resistivity
TMI	Total Magnetic Intensity